CHAPTER 6

PHOSPHIDE NANOWIRES FOR PHOTOCATALYTIC APPLICATION

6.1 Introduction

Green and *Clean Energy* is the only hope to save the ecosystem from hazardous and non-advantageous energy producing and utilizing activities. There is no doubt about the markable progress made in the recent decades, but it is to be agreed that during this technological revolution, the mankind has disturbed natural activities and affected the balance of the eco-system. Hydrogen being the lightest, yet markedly efficient has been realized as the clean source of energy, and the production of hydrogen being one of the latest green energy application fields has driven great attention of research community to improve the non-conventional water-splitting catalysts.[1] Breaking of water-molecule is known as water-splitting process, and the materials associated to increase its rate is known as a catalyst. The water-splitting is a two-step process, the one being the hydrogen evolution reaction (HER) and other as oxygen evolution reaction (OER), the corresponding catalysts can be termed as HER or OER catalysts respectively.[2] The chemical reactions taking place during these processes are shown below:

$$2H^+ + 2e^- \rightarrow H_2 \quad (6.1)$$

and

$$2H_2O \rightarrow O_2 + 4\,H^+ + 4e^- \quad (6.2)$$

Yielding overall reaction, $2\,H_2O \rightarrow 2\,H_2 + O_2$ (6.3)

The HER mechanism can be further viewed in form of two sub-steps, the first in which the H^+ gets adsorbed on the surface of the catalyst known as Volmer step which is then followed by the second stage known as Heyrovsky or Tafel steps.[2] Extremely

expensive metals like Platinum (Pt), Palladium (Pd), Gold (Au) and Silver (Ag) have been utilized as the catalyst, with Pt being most expensive yet recognised as the best catalyst;[3] although many efforts of the researchers are converged to develop a catalytic material, that not only possesses markable electronic and catalytic responses, but also are eco-friendly in nature, abundant in quantity and cost-effective.[4–6] In this regard, the III-V materials due to their unique electronic dispersions and robust nature have been utilized for many cutting-edge technologies like spintronics,[7] nano-electronics,[8] optoelectronics[9,10]but very scares data are available on their application as a water-splitter catalyst under nanostructured configuration.[11–13]Apart from material selection and nanostructuring, methods like heterostructuring,[14,15] external strain[16,17] and doping[18] are also being used for tuning the intrinsic nature of the materials. In present chapter, two ultra-thin phosphide-based nanowires (NWs) namely boron phosphide (BP) and gallium phosphide (GaP) NWs are considered for investigating their structural, electronic and catalytic properties.

6.2 Computational Details

The NWs are investigated within the *state-of-art* density functional theory (DFT).[19] Prior to computation of electronic and catalytic properties, the individual NWs were constructed by supercell approach using the respective bulk unit cells[20] and then were optimized till the total-energy of the systems did not reach its minima. The description of the atomic species was done by means of employing norm-conserving type local density approximated pseudopotentials[21] that are known to give better prediction of ground state properties for III-V compounds.[22] The kinetic energy cut off for the electronic wave-function was set to 680 eV for both NWs. The integration of Brillouin

zone was done within the well-converged Γ-centred Monkhorst-Pack scheme[23] based k-mesh of density 1x1x10. The convergence thresholds for total energy and forces as 10^{-6} eV and 10^{-3} eV/atom, respectively were set for achieving reliable predictions. For accurate prediction of the surface edge states and adsorption profiles, the unsatisfied surface atoms of the NWs were saturated by passivating the NWs with hydrogen adatoms. Furthermore, the long-range Coulomb interactions were treated by including van der Waals correction to the ground state DFT calculations.[24] Followed by the well-optimized structures, the NWs were considered for computing the ground state electronic properties followed by the adsorption profiles. The adsorption energy was computed by aligning the adsorbate atom ~ 3 Å apart from the target surface site and was then allowed to get fully relaxed keeping all necessary parameters fixed. After complete relaxation, the ground-state energies of the respective systems were considered and adsorption energy was computed (see Equation 6.4):

$$E_{ads}^{NW} = E_{Complex}^{H/O-NW} - E^{NW} - E_{H/O} \qquad (6.4)$$

The terms $E_{Complex}^{H/O-NW}$, E^{NW} and $E_{H/O}$ represent the energies of the hydrogen/oxygen adsorbed pristine/doped NW, pristine/doped NW without adsorption and half of the energy of isolated hydrogen/oxygen molecule.

$$\Delta G_{H/O} = \Delta E_{H/O} + \Delta E_{ZPE} - T\Delta S_{H/O} \qquad (6.5)$$

The term ΔE_{ZPE} which lies within the range 0.0 to 0.04 eV[25–27] for hydrogen and is nearly zero for oxygen,[27] is the zero point energy difference of hydrogen/oxygen in adsorbed state and gas phase, and the third term $\Delta S_{H/O}$ is the difference in the entropy of hydrogen/oxygen under adsorbed state and gas phase, and under experimental

conditions, the value of $T\Delta S_{H/O}$ is about 0.4 eV for hydrogen,[26,27] and for oxygen, the entropies of adsorbed and gas phases are zero and 0.631 eV, respectively.[26] Considering the reported magnitudes, the terms ΔE_{ZPE} and $T\Delta S_{H/O}$ reduce to 0.24 or 0.33 for the case of hydrogen or oxygen adsorption, respectively. The effect of hydrogen/oxygen adsorption on electronic transport properties is also assessed by re-computing the PDOS of the NW after subjecting to hydrogen/oxygen adsorption on different adsorption sites.

6.3 Results and discussion

6.3.1 Boron Phosphide Nanowire (BP NW)

6.3.1.1 Structural Properties

As discussed in the **Computational Details** section, the ultra-thin boron phosphide nanowire (BP NW) was constructed from the optimized bulk unit cell and then was again well-optimized independently so as to achieve ground state configuration with minimum total-energy. The optimized crystal structure of the BP NW is presented in Figure 6.1, and corresponding parameters are listed in Table 6.1. As it can be observed from the Table 6.1, the optimized lattice parameter of the bulk BP is in agreement with the reported data;[28] however, in case of BP NW, there are no experimental reports to compare with, although, the anion-cation bond distances and angles can be considered for getting a comparative assessment. It is observed that in the case of bulk BP, the cation-anion angles are same and consistent in all directions; whereas, in the case of BP NW, the cation-anion angles show deviation of 5°. This might be the result of inclusion of hydrogen adatoms on the NW surface that reassemble themselves and

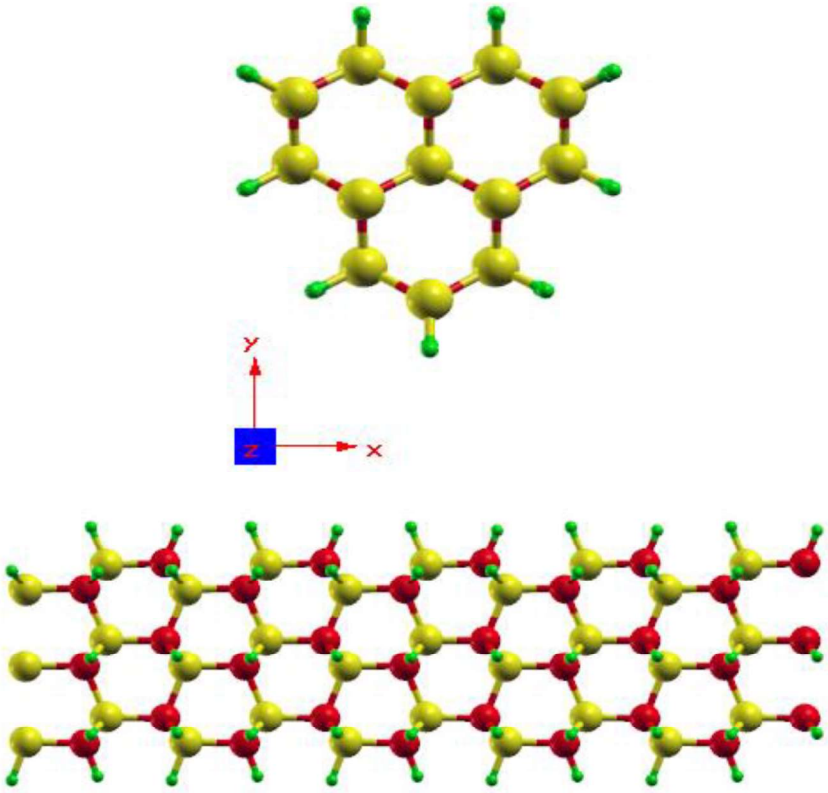

Figure 6.1. Top and Side views of optimized crystal structure of pristine BP NW (atoms in yellow, red and green represent boron, phosphorous and hydrogen atoms, respectively).

the surface atoms in such a way that the total-energy of the system is minimized. As it can be viewed from the Fig. 6.1(a), the hydrogen adatoms have settled in a buckled geometry so as the surface energy of the system minimizes. For assessing the stability of the NW, the formation energy of the BP NW has been computed using the equation given below:

$$E_F^{NW} = \frac{E_{Tot}^{NW} - m\mu_B - n\mu_P - l\mu_H}{m+n+l} \qquad (6.6)$$

Where, the terms E_F^{NW} and E_{Tot}^{NW} represent the formation and total-energy of NW, respectively and, μ_B, μ_P and μ_H are the chemical potentials of the boron, phosphorous and hydrogen with their respective number of atoms symbolized as m, n and l in the

NW unit cell. The computed formation energy of the NW is found to be -5.61 eV; wherein the negative sign and low magnitude indicate that the NW is stable and the formation is exothermic in nature.

Table 6.1. Computed structural parameters of WZ BP in bulk and NW configurations.

System	No. of Atoms B/P/H	Lattice Parameter C (Å)	Bond Length (Å)			Angle		Formation Energy (eV)
			B-P	B-H	P-H	B-P-B	P-B-P	
BP (bulk)	2/2/0	5.225	1.94	-	-	109.2°	109.2°	-
BP (NW)	13/13/18	5.257	1.93	1.21	1.41	109.9°	104.7°	-5.61

6.3.1.2 Electronic Properties

For getting insight to the electronic transport of the BP NW, and to assess the spatial distribution of individual electronic orbitals of the constituent atoms within the first Brillouin zone limit, the electronic dispersion curves and the total and partial electronic density of states (DOS and PDOS) are computed (see Fig. 6.2 and Table 6.2). Apart from the pristine NW, the effect of substitutional defect/doping is also addressed (see Fig. 6.3 and Table 6.2).

Table 6.2. Electronic band gap (E_g), electron effective mass (m_e^*) and nature of band gap of Boron Phosphide in bulk and NW geometries.

System	E_g eV	$m_e^*(m_0)$	Nature
BP-bulk	0.84	0.41	Indirect
BP-NW	2.96	9.74	Direct
BP-Al NW	2.81	4.37	Direct
BP-Ga NW	2.87	5.04	Direct

As it can be observed from the Fig. 6.2(a), the location of the valence band maxima (VBM) and conduction band minima (CBM) is lying at the centre of the Brillouin zone (Γ point) indicating direct nature of the electronic band gap, similar to the report on WZ GaP NW,[29] but is in contrast to other NWs from the same family.[16,17] As expected, the gap magnitude in present case is found to be 2.96 eV (see Table 6.2) higher than the bulk BP subjected to quantum confinement effect. Furthermore, akin to the other III-V compounds, the indirect nature of the gap in case of bulk BP is observed to get transformed into direct on imposing two-dimensional confinement.[29,30]

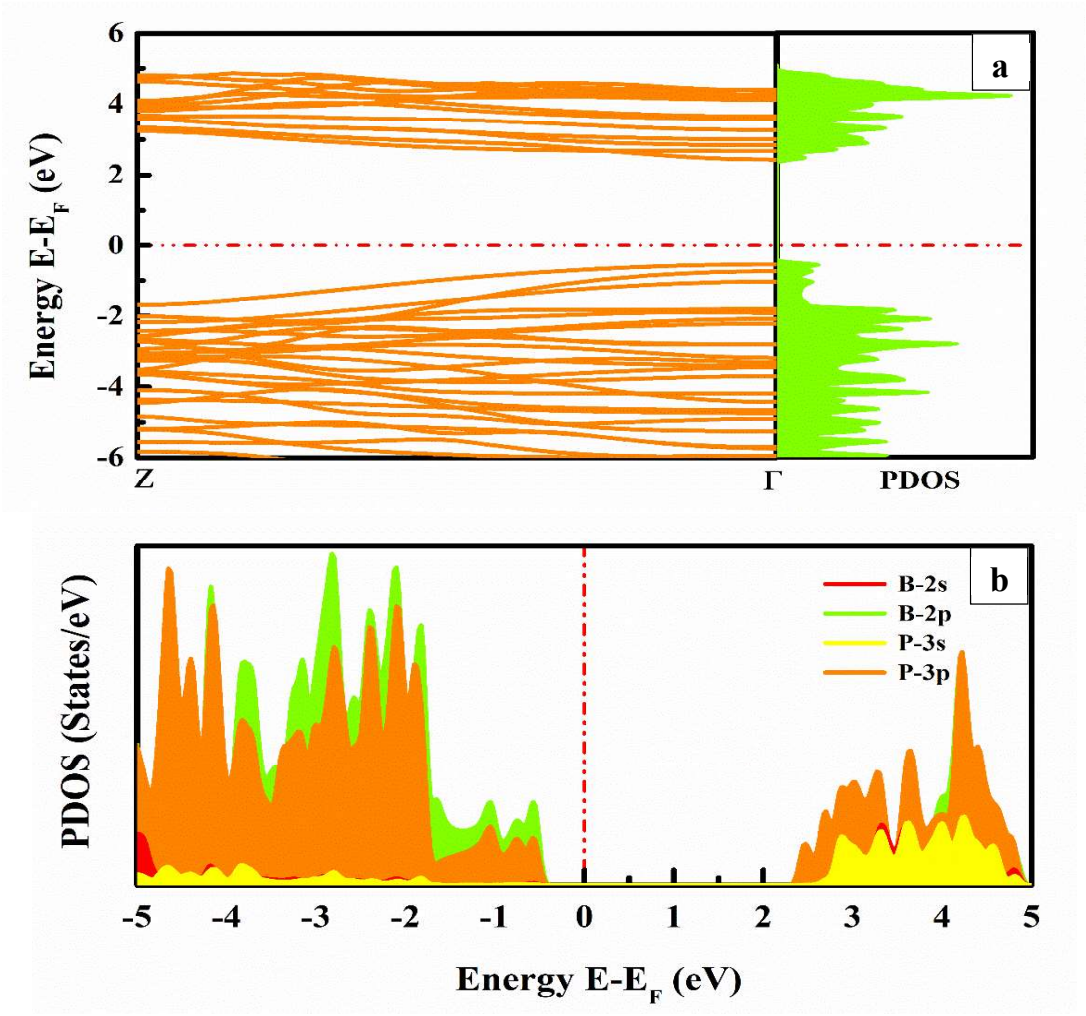

Figure 6.2. (a) Electronic Band Structure with corresponding density of states (DOS) and (b) partial electronic density of states (PDOS) of BP NW.

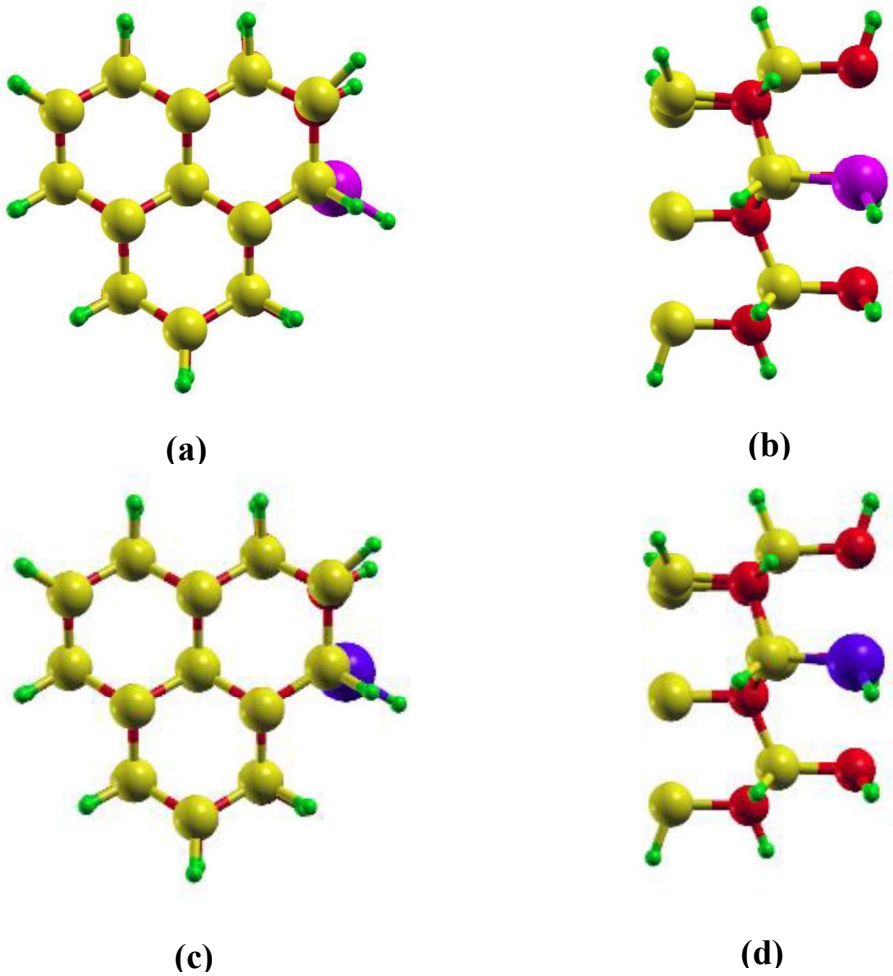

Figure 6.3. Top and side views of BP NW doped with aluminium (a, b) and gallium (c, d) respectively (atoms in purple and blue are aluminium and gallium, respectively).

The term effective mass is related to the dynamic mass of the charge carrier, which strongly depends on the position of the carrier and the considered direction of the carrier transport in the crystal. Considering the above two facts, we have tried to understand the dimension dependent carrier effective mass, and for this, the electron effective mass for bulk and NW systems in 0001 direction is computed (see Table 6.2) by extracting the edge states from the respective electronic band structures and fitting them with second order polynomial. From the computed values of effective masses, it

can be concluded that the subjected to gigantic modifications in the transport properties of the system the electron effective mass show rapid enhancement due to confined geometry. Further, substitution of other group-III element in place of boron results in decrease of gap from 2.96 eV for pristine NW to 2.81 eV and 2.87 eV for Al and Ga doped BP NWs, respectively keeping the bandgap nature unaltered. The PDOS plot presented in Fig. 6.2(b) replicates the contribution of different atomic orbitals to the electronic properties in form of characteristic van Hove singularities. As observed, the *3p-orbital* of the phosphorous atom dominates in the CBM whereas, its contribution to the VBM regime is almost equal to that of boron atom's *2p-orbital*. The significant contribution of *3s-orbital* of phosphorous atom is observed in CBM regime. Further, the orientation of Fermi energy lying near the VBM regime replicates the *p-type* semi-conducting nature of the BP NW.

6.3.1.3 Catalytic activity of BP NW

Moving towards the main goal, the overall catalytic activity of BP NW is assessed through computing the surface adsorption energy of the NW subjected to the hydrogen or oxygen for studying the hydrogen evolution reaction (HER) and oxygen evolution reaction (OER) activities. The overall assessment of the HER and OER activities is assessed in the vicinity of the adsorption and Gibbs free energy.

6.3.1.3.1 Hydrogen Evolution Reaction (HER) Activity

As mentioned, hydrogen is the cleanest source of energy and one of the best ways to produce/obtain clean energy by breaking water molecules in to its constituent hydrogen and oxygen molecules. The so-called process of water-splitting is the green and clean way for producing hydrogen that can be utilized as a fuel to generate

electricity. To carry out the HER activity at ambient conditions, the time and production rate are not feasible; and to overcome this, the materials that can act as catalysts are utilized which just modify the reaction rate without participating in the reaction. The conventionally utilized catalyst for this purpose is made up from the expensive metals like Pt, Pd, Au etc., which are not feasible at large scale owing to their production expenditure. To overcome this disadvantage, we need to design/engineer materials with required catalytic activity and low production rates.

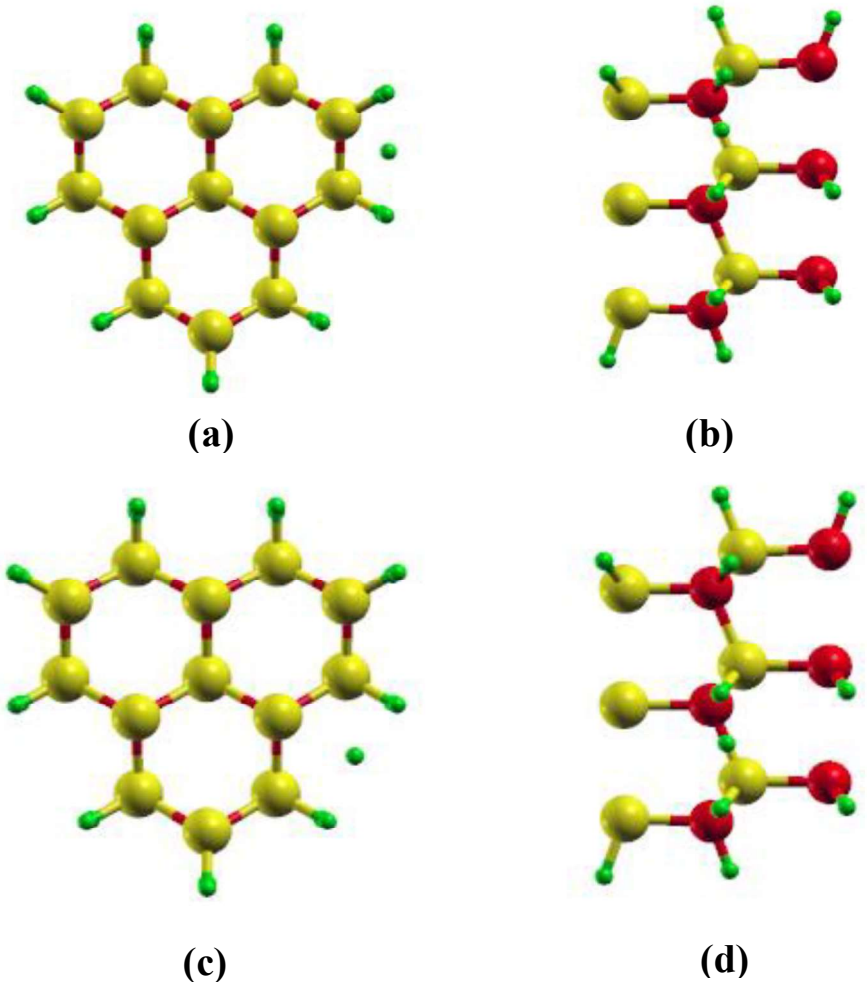

Figure 6.4. Top and side views of BP NW with hydrogen adsorbed on two distinct surface sites (a, b) Site-A and (c, d) Site-B.

For this purpose, materials like BP acquiring much more portion of earth's crust than the conventional expensive metals are being studied for assessing its performance as HER catalyst.

To assess the HER activity of BP NW, we have adsorbed the H atom (green coloured atom) on two distinct sites of the NW surface. The top and side views of the BP NW prior to complete hydrogen adsorption are presented in Figure 4(a-b). As can be seen from the figure, two distinct bridge sites of the NW surface are selected for studying the HER activity. The interaction of hydrogen with NW surface was analysed by fully relaxing the NW after adsorption of hydrogen; the final geometry of the NW subjected to hydrogen adsorption is depicted in Figure 6.5, wherein, the Figs. 6. 5(a), (b) and (c), (d) are the top and side views of BP NW with hydrogen adsorbed on site-A and site-B, respectively. Furthermore, the modification in the cation-anion distances and angles subjected to hydrogen adsorption are tabulated in Table 6.3.

Table 6.3. Computed bond lengths and angles of BP NW subjected to hydrogen adsorption at different sites of NW surface.

Configuration	Bond Length (Å)			Angle		D (Å)
	B-P	B-H	P-H	P-B-P	B-P-B	H-NW
Site-A	2.89/1.94	1.23	1.42	83°/106.4°	119.6°/110.4°	1.22
Site-B	2.11/1.95	1.21	1.43	106.9°/105.4°	103.3°/110.4°	1.55

For better HER activity, it is desired to have a catalyst that does not over bind the hydrogen so as to make desorption step possible, else the target of energy generation cannot be achieved. As it can be observed from Figs. 6.5 (a, b) and Table 6.3, while hydrogen is introduced on site-A of the NW surface, it gets adsorbed on the surface

of the NW through chemisorption process and strongly binds with the surface cation. The chemisorption of hydrogen causes perturbation in the NW surface geometry, which can be clearly seen in Figs. 6.5(a, b). The observed B-P bond length near site-A which was 1.93 Å in case of pristine NW gets elongated to 2.89 Å and the corresponding angles B-P-B and P-B-P are modified to 119.6° and 83° from 109.9° and 104.7°, respectively. The corresponding computed adsorption and Gibbs free energy of the system is found to be -1.4 and -1.19 eV, respectively which replicates that the HER activity of BP NW lies within feasible range. However, in the second case,

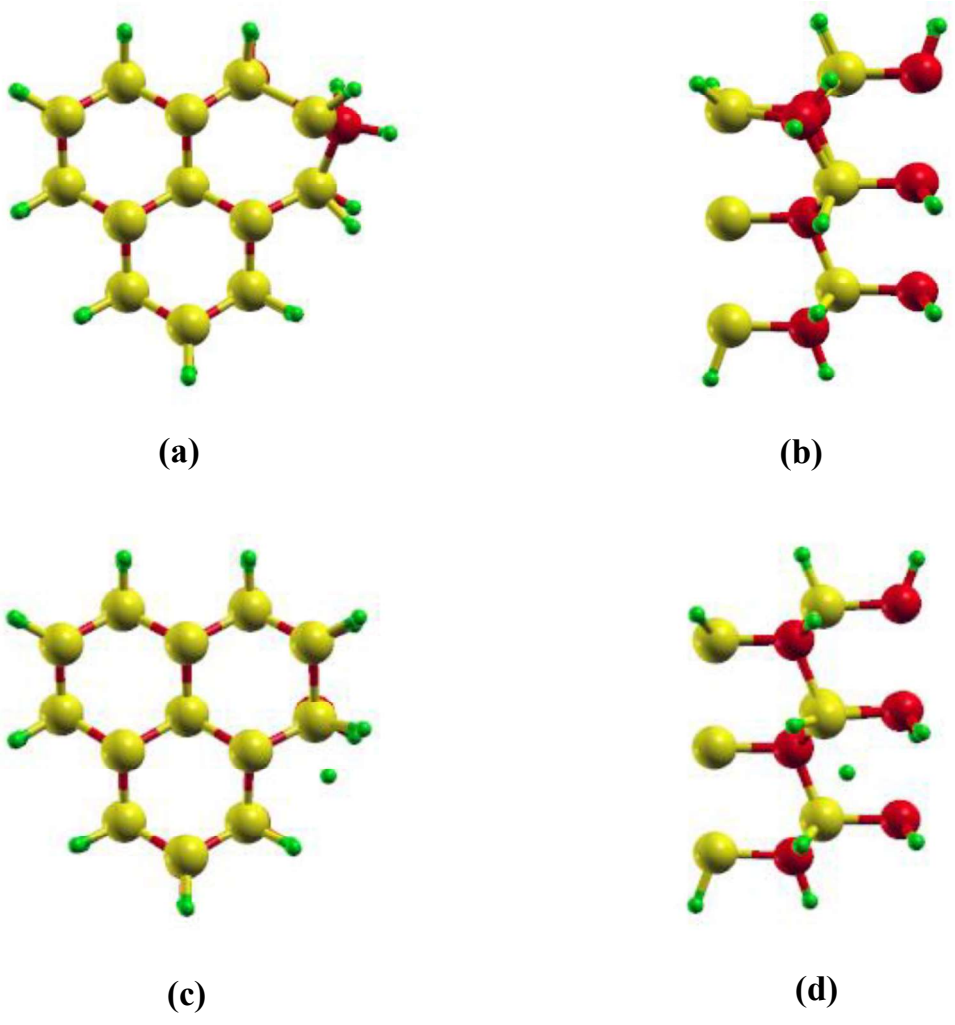

Figure 6.5. Top and side views of BP NW subjected to hydrogen adsorption on Site-A (a, b) and Site-B (c, d) respectively.

wherein the hydrogen is adsorbed near the concave surface of the BP NW, we found totally different adsorption response.

The B-site of the NW is found to be more suitable for adsorption due to physisorbed ion of hydrogen on the NW surface (see Figs. 6.5(c, d)) without any chemical bond formation between the adsorbent and adsorbate. There is almost negligible perturbation in the surface geometry of the NW compared to the A-site adsorption. This observation can be confirmed by the anion-cation distances and angular

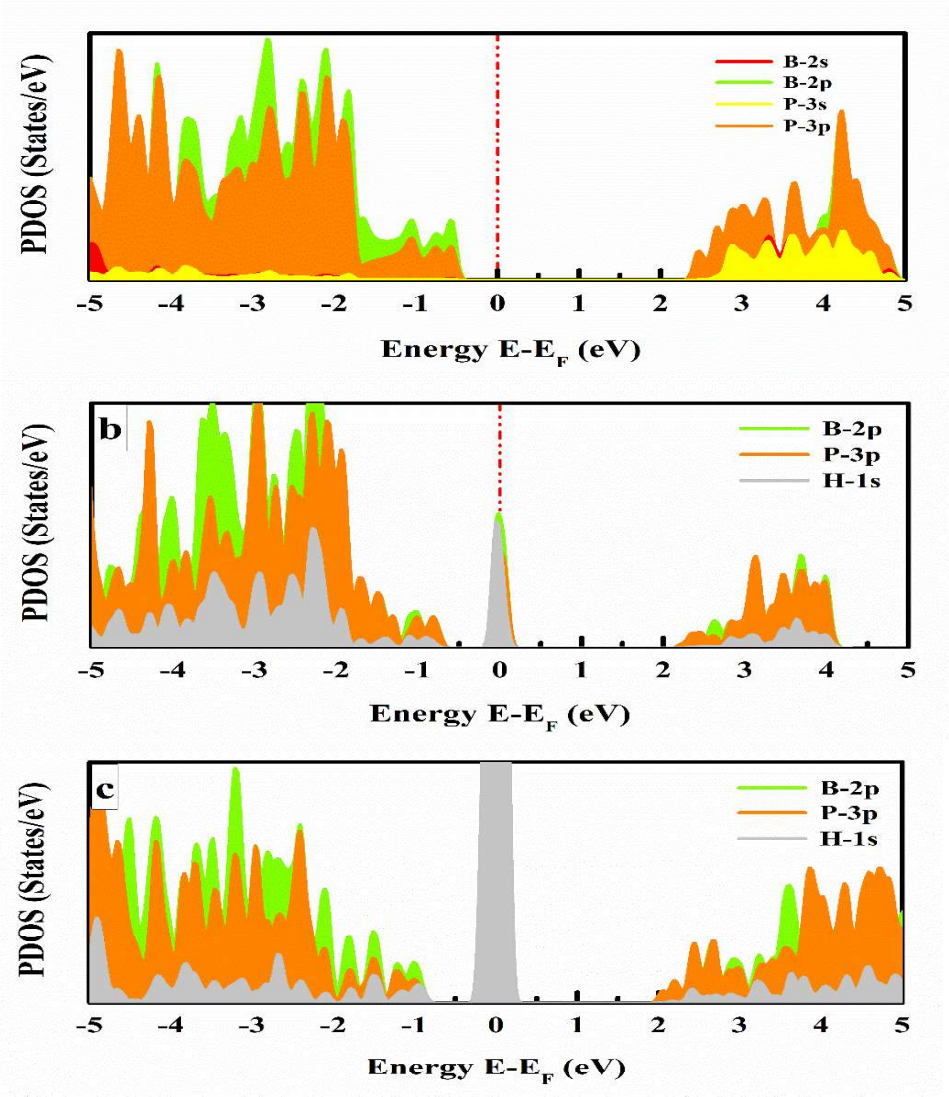

Figure 6.6. Partial density of states (PDOS) of BP NW in (a) pristine and, H adsorbed on (b) Site-A and (c) Site-B, respectively.

magnitudes enlisted in Table 6.3, which are almost similar to that of the pristine NW. Furthermore, the energies of adsorption and Gibbs function replicate the better HER activity of BP NW in this case with values of -1.07 and -0.83 eV, respectively. Henceforth, we conclude that the B-site is the most preferred site for hydrogen adsorption keeping the geometry and morphology of the adsorbent unperturbed with desirable magnitudes of adsorption and Gibbs free energies.

To understand the modifications in the electronic transport of BP NW subjected to site dependent hydrogen adsorption, we have computed the partial electronic density of states (PDOS). The graphical comparison of computed PDOS for pristine and H-adsorbed BP NW is depicted in Figure 6.6. As it can be clearly observed from Figs. 6.6 (a), (b) and (c) that the pristine NW possesses finite electronic bandgap with moderate value of 2.96 eV. However, when hydrogen is introduced in the system at A-site (see Figs. 6.5(a, b)), the VBM and CBM states get markedly modified and excess states at Fermi level are observed because of chemisorbed hydrogen. The modification in the hybridized states of BP NW results in metallic nature of the adsorbent. On the other hand, the adsorption of hydrogen at B-site results in much more pronounced electronic states at Fermi level showing enhancement in metallic character of the adsorbent. After unravelling the complete picture on hydrogen adsorption on two distinct sites of BP NW surface, we tried to understand the effect of substitutional doping on the hydrogen adsorption properties. The results on adsorption energy and Gibbs free energy show that the Al and Ga atoms on B site of the NW increases the magnitude of the adsorption and Gibbs energy thereby suggesting that the substitutional defects may significantly affect the catalytic properties of the material.

Therefore, in the present case, compatibility of BP NW as an HER catalyst reduces under modified chemical environment (see Table 6.5).

6.3.1.3.2 Oxygen Evolution Reaction (OER) Activity

For estimating over-all catalytic activity of BP NW for water-splitting, besides HER activity, we have also computed the oxygen evolution reaction (OER) activity of NW by adsorbing oxygen on two different sites of the BP NW surface (see Figure 6.7).

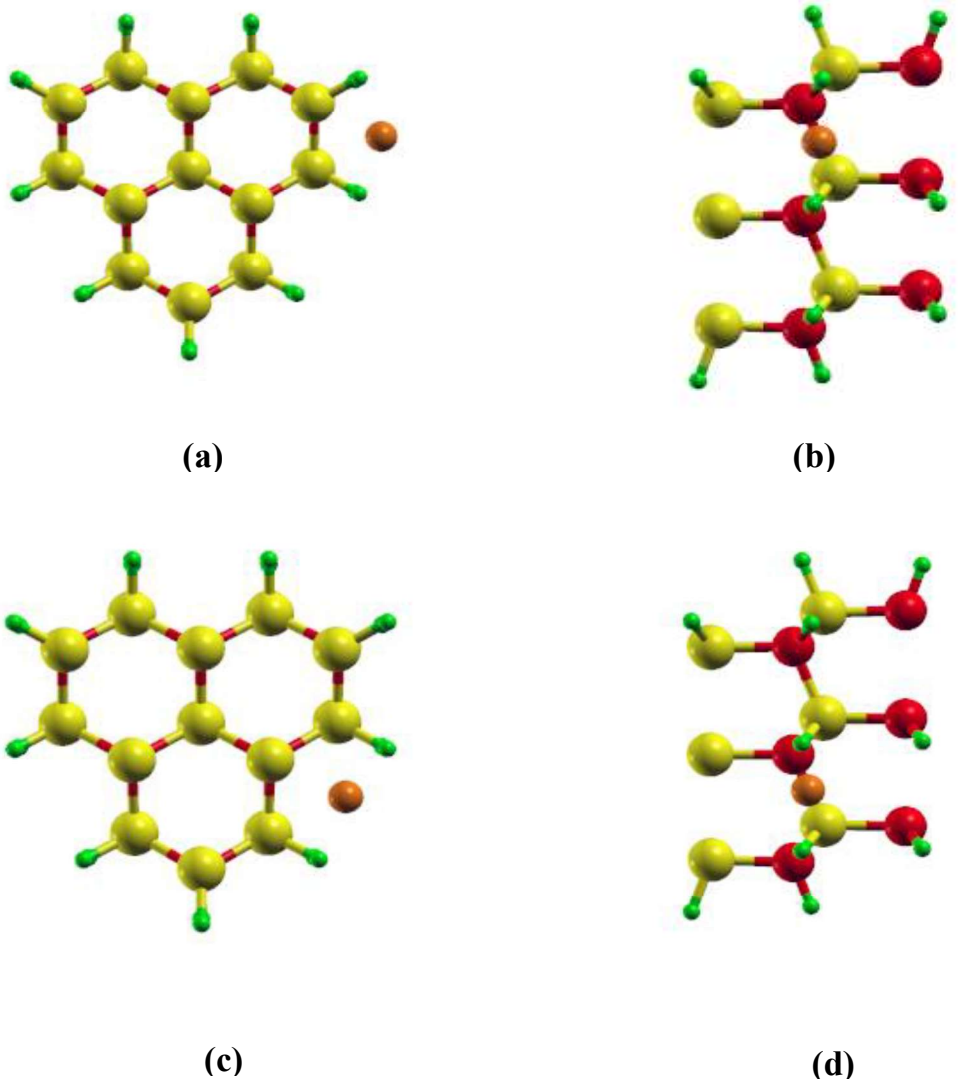

Figure 6.7. Top and side views of BP NW before adsorbing oxygen atom on site-A (a, b) and site-B (c, d) respectively.

Similar to hydrogen adsorbed NW, the adsorption and Gibbs free energies in this case were computed using equations (1) and (2) respectively and the corresponding values with modified bond-lengths and angles are presented in Table 6.4. Figs. 6.7 and 6.8 represent the top and side views of the BP NW before and after oxygen adsorption on two distinct sites. We observe that after adsorption, the oxygen atom in both cases migrates towards the NW surface and finally through chemisorption process, gets attached with the boron atom in case of A-site and phosphorous atom in case of B-site by displacing the surface hydrogen atom (see Fig. 6.8). The computed adsorption and Gibbs free energies of BP NW for oxygen adsorption over A-site are -8.26 and -7.93 eV and -8.31 and -7.98 eV for B-site, respectively. These magnitudes are too negative and show strong bonding between oxygen and adsorbent. Further, the angles between so-formed oxygen centred geometry is 112.9° (B-O-H) and 109.2° (P-O-H) for sites A and B, respectively. It is noteworthy that the cation-anion bond lengths in both cases are slightly modified as compared to pristine NW, but the cation-anion angle in case of B-site shows significant increase. Further, the observed O-H bond lengths are 0.97 and 0.98 Å for A and B sites, respectively, which are in agreement with the standard O-H bond length (0.98 Å).[31]

Table 6.4. Computed bond lengths and angles of BP NW subjected to oxygen adsorption on different sites of NW surface.

Configuration	Bond Length (Å)			Angle			D (Å)	
	B-P	B-H	P-H	P-B-P	B-P-B	B-O-H/ P-O-H	O-NW	O-H
Site-A	1.94	1.21	1.41	103.3°	110.7°	112.9°	1.42	0.97
Site-B	1.91	1.22	1.41	109.8°	110.2°	109.2°	1.61	0.99

The effect of strong bonding between oxygen and the adsorbent on the electronic transport of the system is analysed by computing partial density of states (PDOS). The

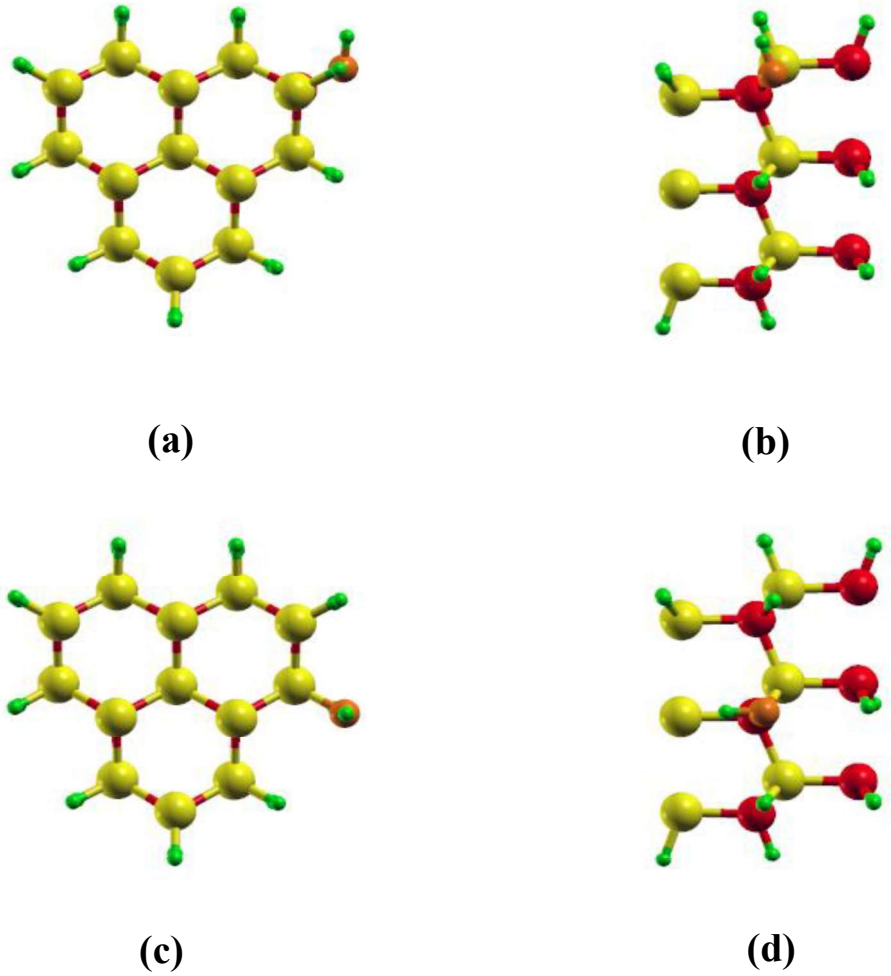

Figure 6.8. Top and side views of BP NW subjected to oxygen adsorption on Site-A (a, b), and, Site-B (c, d) respectively.

PDOS plots of BP NW with oxygen adsorbed on site-A (Fig. 6.9(b)) and site-B (Fig. 6.9(c)) show similar semiconducting behaviour as pristine BP NW, with shift in electronic levels that further modify the electronic band gap from 2.98 eV (pristine) to 2.72 eV (site-A) and 2.77 eV (site-B). The clear splitting of oxygen electronic level into its bonding and anti-bonding states due to chemisorption (see Figs. 6.9(b) and (c)) supports our calculated values of adsorption energy and confirms the presence of

strong bonding between oxygen with the NW. Further, the markable dominance of oxygen bonded atom's *p-orbital* (boron in case of site-A, and phosphorous in case of site-B) in the CBM regime indicates the oxygen atom's key role in electronic transport.

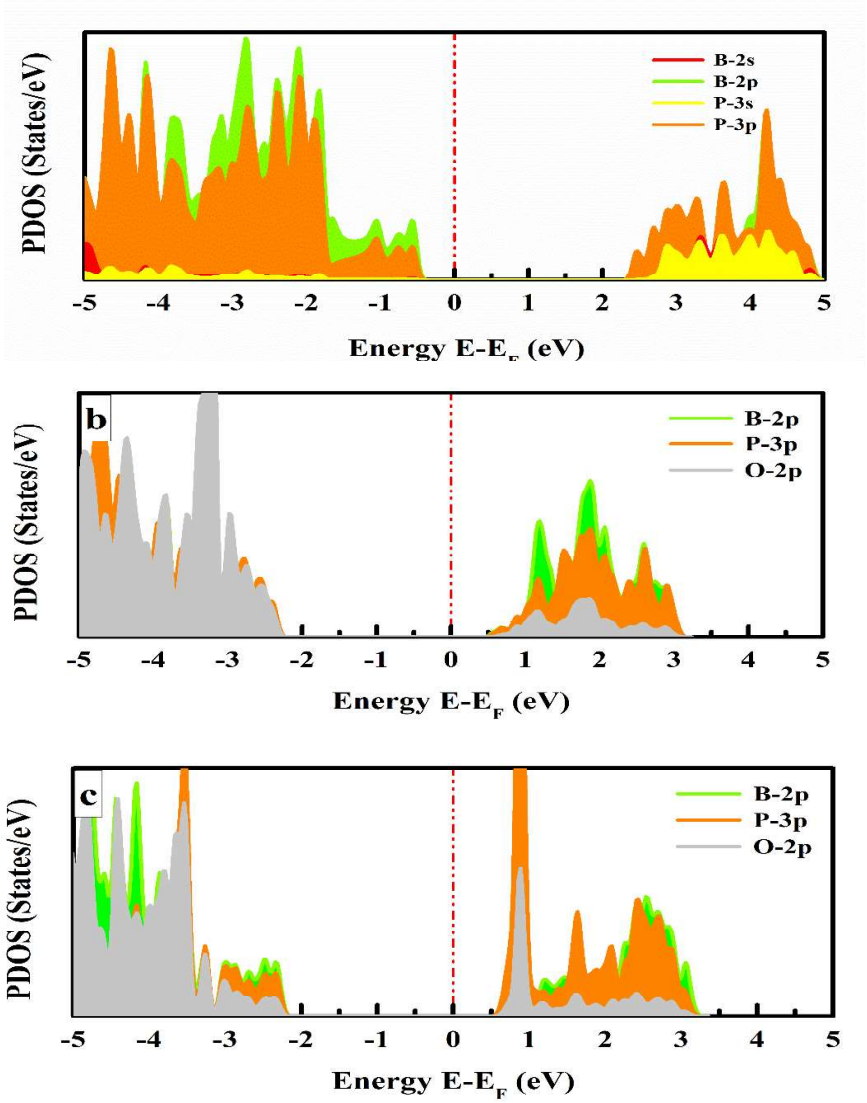

Figure 6.9. Partial density of states (PDOS) of BP NW in (a) pristine and O adsorbed on (b) Site-A and (c) Site-B, respectively.

The shifting of Fermi level form VBM to CBM regime shows dramatic reversal of the electronic nature of the BP NW from *p-type* (pristine NW) to *n-type* (O-adsorbed NW) due to addition of excess electrons to the system. From the results of the adsorption energy and electronic states, we conclude BP NW not to be a good catalyst for water

oxidation, as it over binds oxygen atom making desorption procedure non-feasible and complicated. Further, similar to hydrogen adsorption case, we have also studied the effect on oxygen adsorption properties of BP NW by means of Al and Ga doping. Surprisingly, in this case Al doped NW does not show any considerable modulation in adsorption profile (see Table 6.5). However, in the case of Ga doped at site-B of NW shows a dramatic decrease (~35%) in the adsorption and Gibbs free energies. These results indicate improvement in OER activity of BP NW by increasing Ga concentration and surface site-engineering.

Table 6.5. Adsorption and Gibbs free energies (in electron-volts) of BP NW under hydrogen and oxygen adsorption for pristine and Al and Ga doped configurations.

Hydrogen Adsorption						
NW	BP		BP-Al		BP-Ga	
Site	A	B	A	B	A	B
E(ads)	-1.43	-1.07	-1.94	-1.61	-1.96	-1.40
E(Gibbs)	-1.19	-0.83	-1.70	-1.37	-1.72	-1.16
Oxygen Adsorption						
NW	BP		BP-Al		BP-Ga	
Site	A	B	A	B	A	B
E(ads)	-8.26	-8.31	-8.30	-8.033	-8.28	-5.28
E(Gibbs)	-7.93	-7.98	-7.97	-7.70	-7.95	-4.95

6.3.2 Gallium Phosphide Nanowire (GaP NW)

After investigating the electronic and catalytic activity of the BP NW, we now focus on the properties of the ultra-thin GaP NW.

6.3.2.1 Structural Properties

Similar to the BP NW, the GaP NW was also constructed from the optimized bulk unit cell and the structural parameters of the NW were re-optimized so as to achieve minimum total energy. It can be observed from the optimized configuration of the

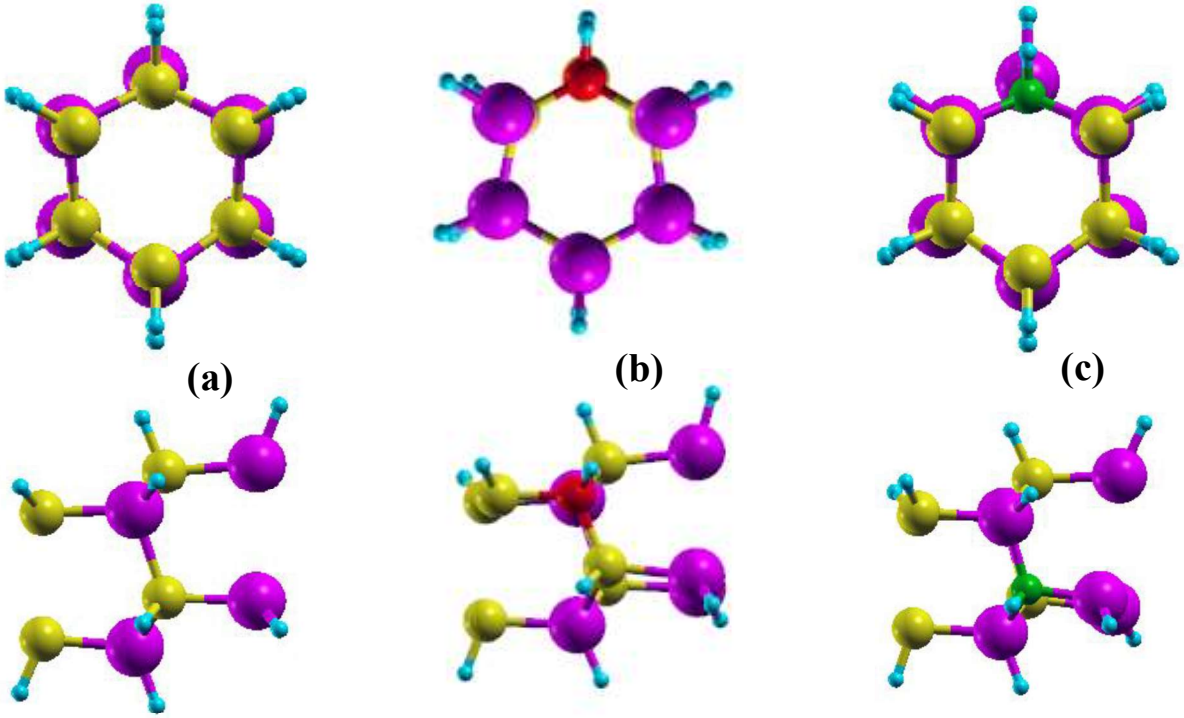

Figure 6.10. Cross sectional view (upper panel) and side view (lower panel) of Gallium Phosphide nanowire (a) Pristine NW (b) B-substituted NW and (c) N-substituted NW (atoms in purple, yellow, red, green and cyan represent respectively the atoms of gallium, phosphorous, boron, nitrogen and hydrogen).

GaP NW (see Fig. 6.10), that the anions and cations are assembled in such a way that the equilibrium is achieved and the NW surface energy is minimized. Unlike the unpassivated NWs,[16] the present NWs show equally distributed cation-anion arrangement. The reason of difference in the positions of anion-cations in case of unpassivated NWs is that the unsaturated valencies of the surface atoms of the NW induce the surface dangling bonds that are usually responsible for false or pseudo edge states, and also may cause reduction in the structural stability of the NW. On the other hand, the balancing of the coulomb forces between the atomic species subjected to incorporation of the pseudo hydrogen atoms in case of passivated NW results in the evenly positioned atoms throughout the NW surface. Furthermore, the inclusion

of the van der Waals correction[24] to the DFT[19] calculations well-defines the system interactions and provides better estimates of the energetics of the system.

As mentioned earlier, it is a rigorous task to grow a defect free crystal structure, and more often the nano-structures are prone to acquire defected configuration. To address this issue, the effect of substitutional defect on the properties of the GaP NW has been assessed by means of selecting lighter Boron (B) atom (having the same valence electrons as Gallium (Ga)) for replacing the heavier Gallium atom (Fig. 6.10(b)) while as shown in Figure 6.10(c), the lighter Nitrogen (N) atom (pentavalent) is considered for substituting one of the Phosphorous (P) atoms. It is noteworthy, that even after introducing defects, the GaP NW retains its stable configuration. As it is clear from top view of Fig. 6.10, due to inclusion of substitutional defect, minor changes in the cation-anion bond lengths and angles of the system can be observed. In case of B-defected GaP NW, on replacing Ga with B atom, P-B-P angle becomes 107.98° contrast to 103.3° (P-Ga-P angle) for pristine system. This is obvious due to the fact that Boron has the highest electronegativity among group III elements. Also, B-P bond length decreases to 1.93 Å which was 2.3 Å in case of Ga-P for pristine system. Similar behavior is observed for N-substituted GaP NW, in which the Ga-N bond length is found to be 1.94 Å and the Ga-N-Ga angle increases to 121° which was 117.4° (Ga-P-Ga) in the case of pristine NW while P-Ga-P angle decreases to 100°.

6.3.2.2 Electronic Properties

After estimating the structural modifications of the defected GaP NW, the electronic band structure calculations of the systems were performed under reduced zone scheme to understand the electronic profiles of pristine and defected GaP NW. The

importance of electronic band structure calculation is that it provides the insight to understand the electronic properties as well as the moment of electron in any material. In addition, the band structure can be used to find the effective mass of the charge

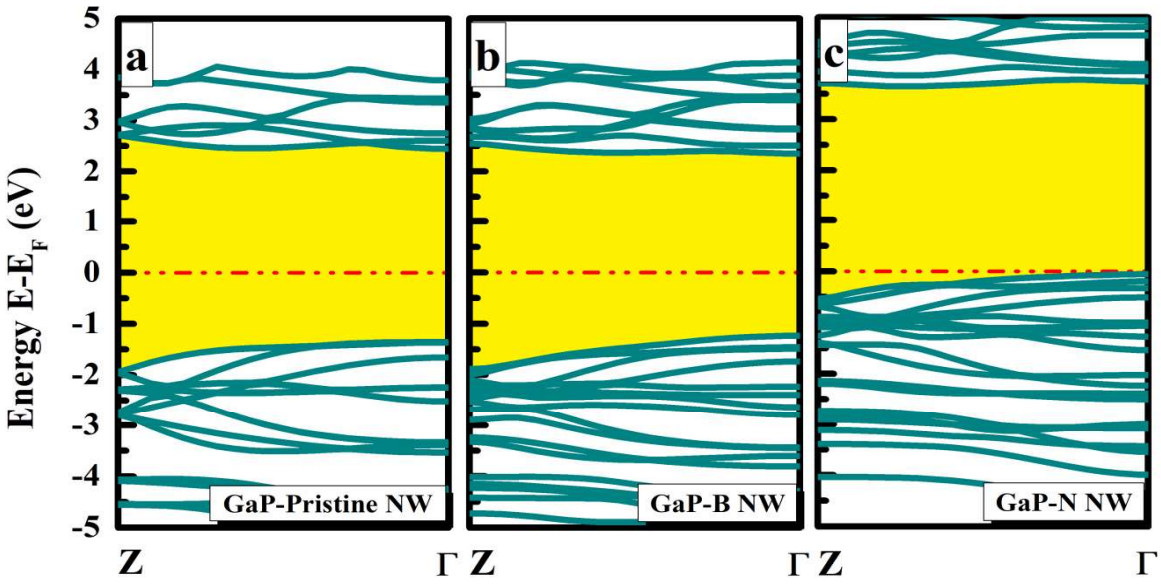

Figure 6.11. Computed electronic band structures of a) pristine, b) Boron defected and c) Nitrogen defected GaP NW.

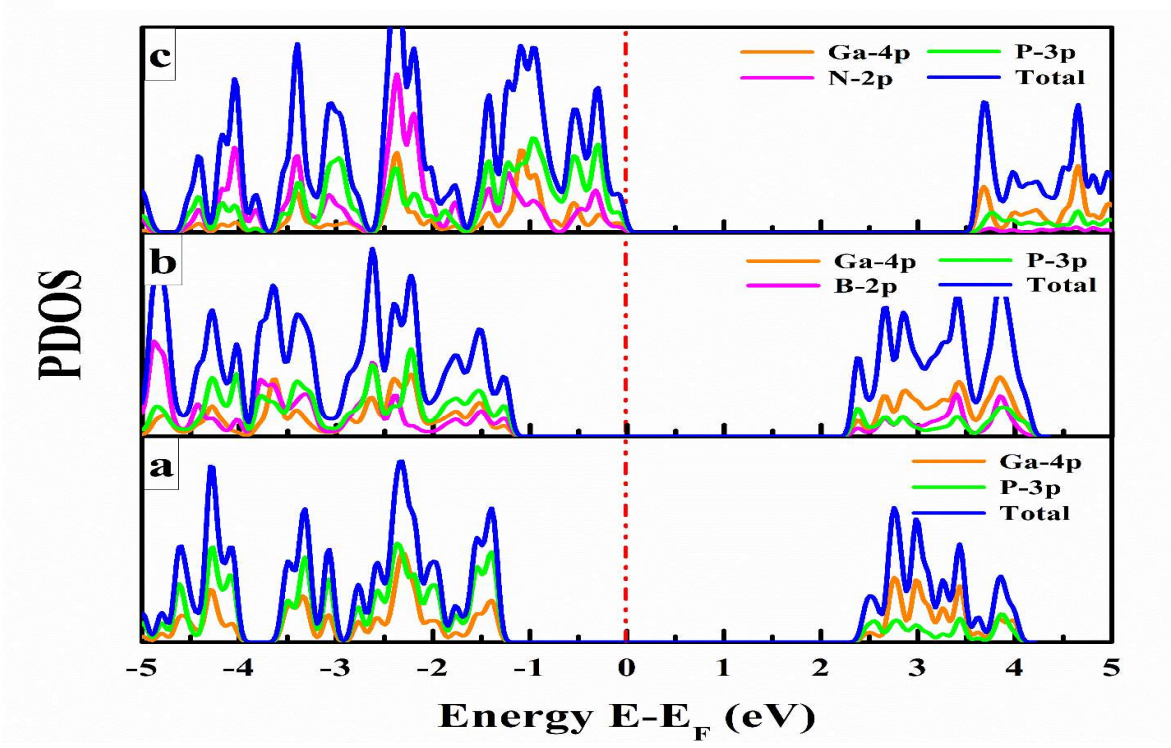

Figure 6.12. Partial electronic density of states of a) pristine, b) Boron defected and c) Nitrogen defected GaP NW.

carriers. The calculated electronic band structures of pristine and defected GaP NWs along **Γ−Z** path are presented in Figs. 6.11 (a-c). It is clear from the figure that the pristine GaP NW is semiconducting with 3.8 eV wide-direct band gap at **Γ** point of the Brillouin zone which is higher than that of bulk and 2D GaP. The bulk GaP has direct band gap of 2.63 eV and indirect gap of 1.96 eV,[20] while 2D GaP has 2.28 eV direct and 1.97eV indirect band gap.[32] The larger band gap in GaP NW can be attributed to the two-dimensional quantum confinement effect. Further, it is observed that the introduction of the defects decreases the electronic band gap of GaP NW. The introduction of B-defect decreases the band gap of GaP NW to 3.58 eV (see Fig. 6.11 (b)), while in case of N atom substitution, the bandgap remains nearly same (3.79 eV), although the valence band maxima (VBM) gets shifted near the Fermi level and the conduction band minima (CBM) towards higher energy (see Fig. 6.11(c)).

For clear understanding of spatial distribution of electronic orbitals of individual atomic species, we have computed the partial electronic density of states (PDOS). The PDOS plots of pristine and defected GaP NW are presented in Figs. 6.12 (a-c) which reveal, that in the case of B-defected GaP NW, the *p-orbital* electrons equally contribute to both band regimes (CBM and VBM). However, in case of N-defected GaP NW, the *p-orbital* electrons create impurity states in VBM closer to the Fermi level. The major concomitant of *p-orbital* electrons of the N atom is observed in the valence band regime of N-defected NW. In general, from the PDOS plots, we conclude that the electronic transport is solely governed by the cations of the system that hold significant contribution in the CBM regime, in contrast to the anions of the system that dominate in VBM regime. In contrary to the observed trend of electronic responses of pristine

GaP NW, the defected NWs show distinct electronic response. For instance, the B-defected NW shows slight modification in the magnitude of electronic bandgap (3.58 eV) which also makes it a potential wide-bandgap semiconductor that can be utilized as a photo-catalyst on further alignment of the electronic dispersion.

6.3.2.3 Catalytic activity of GaP NW

After understanding the electronic properties of the GaP NW, the catalytic activity of the GaP NW towards hydrogen evolution reaction (HER) was assessed by means of adsorbing hydrogen on different surface sites of the GaP NW followed by the computation of the adsorption and Gibbs free energy.

6.3.2.3.1 Hydrogen Evolution Reaction (HER) Activity

For analyzing the most preferred adsorption site of GaP NW, the hydrogen was adsorbed on various sites of pristine GaP NW surface. The adsorption energy and

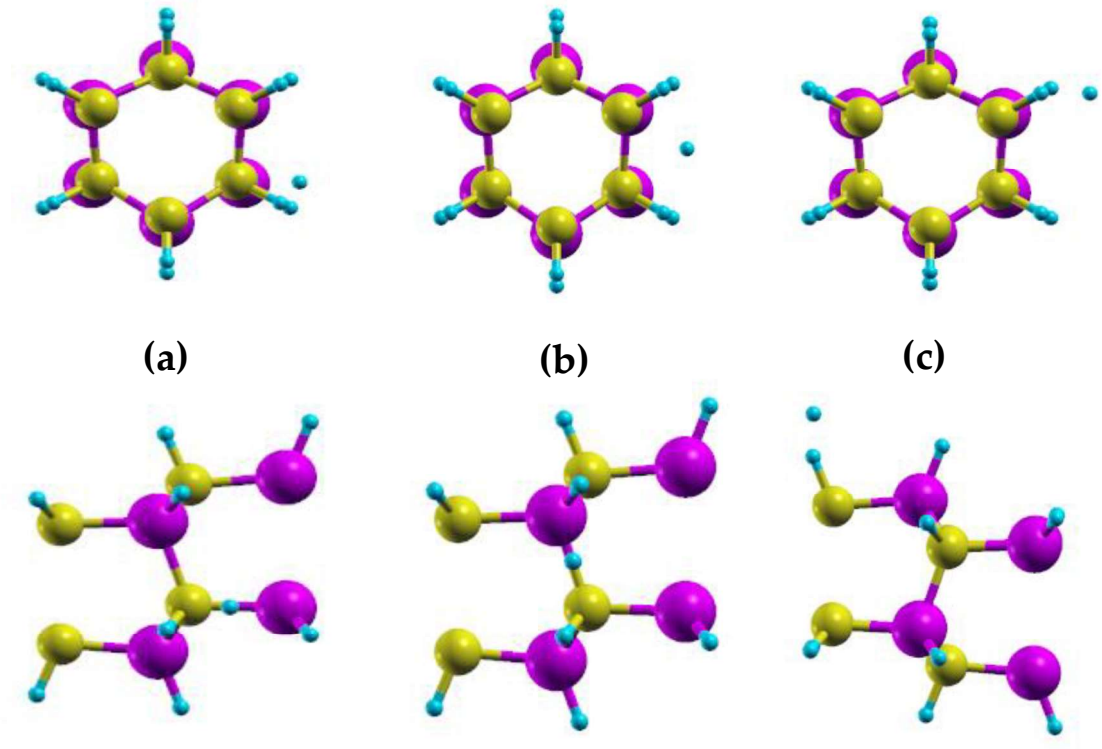

Figure 6.13. Top and Side views of GaP pristine NW before complete adsorption of hydrogen on (a) Site-A, (b) Site-B and (c) Site-C.

Gibbs free energy of the GaP NW were computed using equations (1) and (2) by considering the energies of GaP system and the respective values are listed in Table

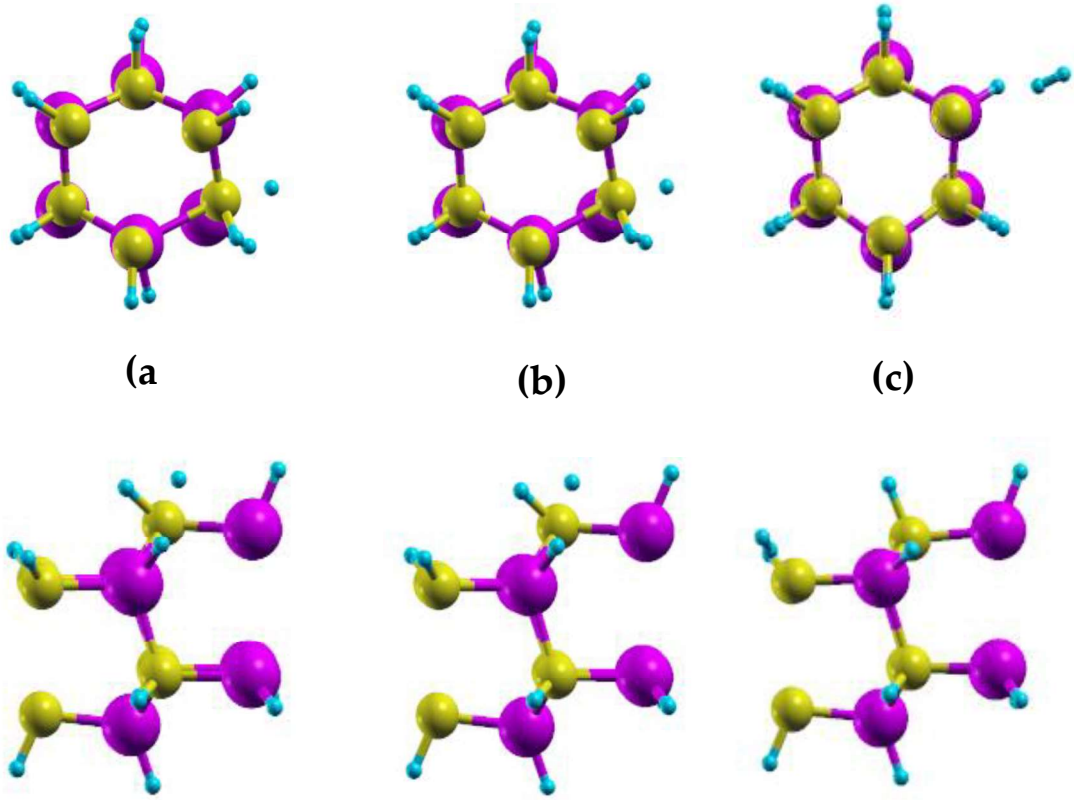

Figure 6.14. Top and Side views of pristine GaP NW after adsorption of hydrogen on (a) Site-A, (b) Site-B and (c) Site-C.

6.6. To visualize the effect of hydrogen adsorption on GaP NW structure, we have presented the top and side views of the pristine GaP NW before and after adsorbing hydrogen on sites-A, B and C (see Figs. 6.13 and 6.14, respectively). From the computed values of adsorption and Gibbs free energies (see Table 6.6) of GaP NW indicate that the Site-A is the most preferred site for hydrogen adsorption and thus was considered for studying the hydrogen adsorption response of GaP NW under defected conditi on.

Table 6.6. Computed adsorption energy, Gibbs free energy and distance between the hydrogen atom to NW surface.

Configuration	Adsorption Energy (eV)	Gibbs Free Energy (eV)	Distance of H atom from NW surface (Å)
Site-A	-1.57	-1.33	1.47
Site-B	-1.58	-1.33	1.48
Site-C	-1.76	-1.52	2.57

After assessing the HER activity of the pristine GaP NW, we now focus on the HER activity of the chemically modified NW. The top and side views of hydrogen adsorbed pristine (a) and defected: (b) B-defected and (c) N-defected GaP NWs are presented in Figure 6.15. As we can visualize, the hydrogen gets adsorbed on the NW surface through physysorption in case of pristine NW, the corresponding adsorption energy is found to be -1.53 eV (see Table 6.7) which indicates good adsorption response of GaP NW for hydrogen atom.

Table 6.7. The computed values of bond-length and distance of adsorbed hydrogen from NW surface.

System	Distance (Å)							
	Ga-P	**B-P**	**Ga-N**	**Ga-H**	**P-H**	**B-H**	**N-H**	**NW surface-H**
Pristine	2.29	-	-	1.53	1.42	-	-	3.53
B-defected	2.34	1.93	-	1.57	1.41	1.21	-	1.57
N-defected	2.29	-	1.94	2.45	1.42	-	1.04	2.45

By introducing B-defect on Ga site in the NW, we observed slight modification in the geometry of the NW (see Fig. 6.15(b)), as the hydrogen gets chemisorbed on the NW surface by making strong chemical bond with Ga atom. The chemisorption of

hydrogen modifies the bond-length of the Ga-P pair of site-A with markable modification in the bond-angle and the energy values (see Tables 6.7 and 6.8).

Table 6.8. Computed bond angles of pristine and defected GaP NW with corresponding adsorption energy.

System	Angle				Adsorption Energy (eV)	Gibbs Free energy (eV)
	Ga-P-Ga	P-Ga-P	P-B-P	Ga-N-Ga		
Pristine	117.5°	103.3°	-	-	-1.53	-1.29
B-defected	121.9°	98.9°	111.33°	-	-1.21	-0.97
N-defected	118.24°	-	-	118.32°	-1.91	-1.67

Our results on N-defected GaP NW are completely different than the one observed for B-defected NW. As observed in Fig. 6.15(c), the adsorbed hydrogen gets attached with the other hydrogen atom present on the NW surface through chemisorption, and at the end detaches the surface hydrogen from N-defected GaP NW. The respective

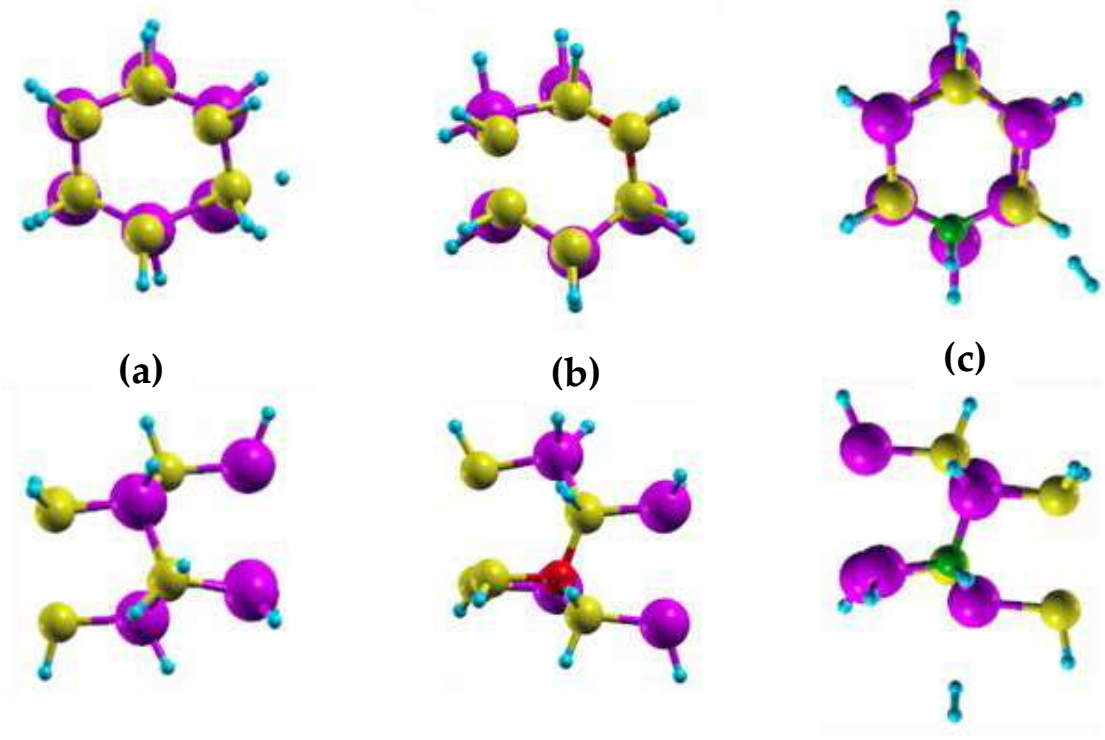

Figure 6.15. Top and side views of a) pristine, b) Boron defected and c) Nitrogen defected GaP NW after adsorbing hydrogen on NW surface.

adsorption and Gibbs free energies are found to be -1.91 and -1.61 eV, are highest observed magnitudes among the considered systems. To analyze the electronic transport through the considered NWs subjected to hydrogen adsorption, we have computed the PDOS for all systems that are depicted in Figure 6.16. Fig. 6.16(a) shows intense peak at Fermi level that is attributed to presence of electronic states indicating semiconductor to metallic transition of pristine GaP NW subjected to hydrogen adsorption. Further, by introducing B-defect on Ga site, the electronic properties get significantly modified (see Fig. 6.16(b)), in turn causing variation in the adsorption response of the NW. The computed value of adsorption energy of B-defected GaP NW is -1.21 eV and the corresponding Gibbs free energy is -0.97 eV which is lowest observed value among remaining systems. We can assert from these results that B-defects improve adsorption profile of GaP NW. Moreover, the significant reduction in

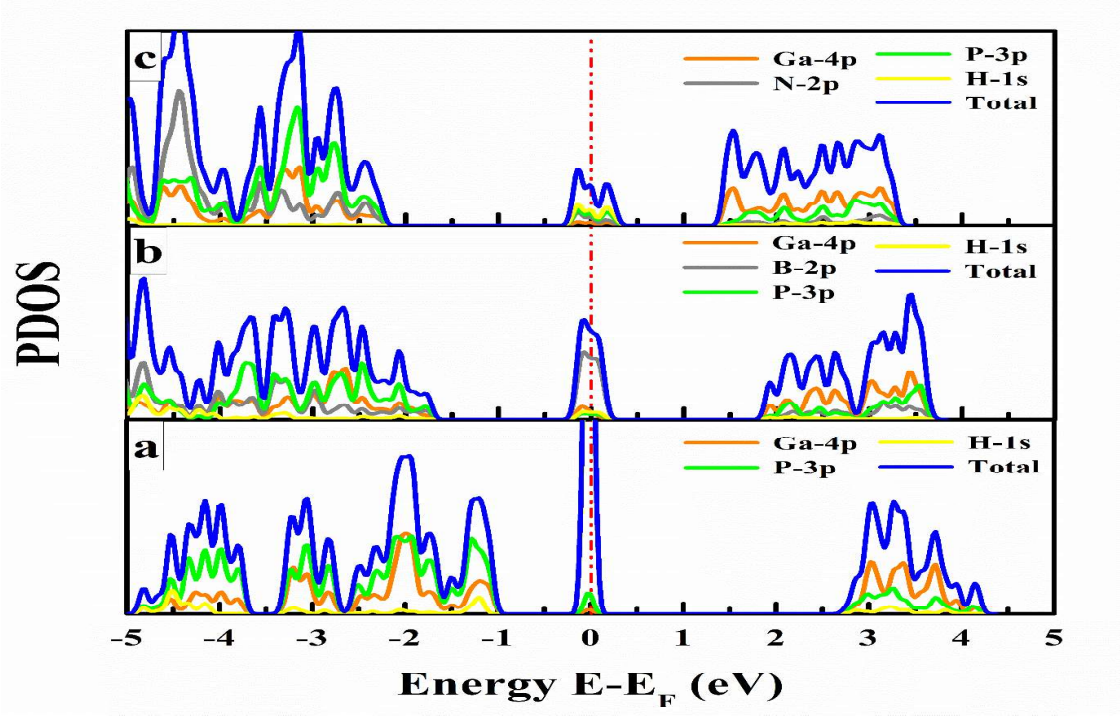

Figure 6.16. Partial density of states (PDOS) of a) pristine, b) Boron defected and c) Nitrogen defected GaP NW after adsorbing hydrogen on NW surface.

density of states at Fermi level (see Fig. 6.16(b)) indicate reduction in metallic nature of the system at the same time showing better adsorption response. Further, by introduction of N-defect in the NW, the PDOS further gets modified as the peak states observed at Fermi level of GaP NW gets much more depressed than the B-defected NW. This observation is in agreement with the computed adsorption energy that is -1.91 eV with corresponding Gibbs free energy of -1.67 eV. These magnitudes implicate that the N-defects might cause reduction in catalyst performance for HER activity under practical conditions. It is evident from the Fig. 6.16, that all systems of GaP NW (pristine and defected), show metallic nature on hydrogen adsorption which is quite favourable and responsible for their enhanced HER activity. The enhancement can be subjected to the contribution of *s-orbital* electron of hydrogen that creates impurity state near Fermi level and as a result, the semi-conducting nature of the systems transforms to metallic.

6.3.2.3.2 Oxygen Evolution Reaction (OER) Activity

Similar to the hydrogen evolution reaction activity, we then investigated the catalytic activity of the GaP NW for oxygen evolution reaction (OER). The computed adsorption energy and Gibbs free energy in this case are -7.38 eV and -7.05 eV, respectively. These magnitudes are too negative and suggest strong binding between the adsorbate and adsorbent which is not preferred for a good catalyst. As in such case, the over binding between the adsorbate and adsorbent causes desorption of the oxygen from NW surface difficult thereby reducing the performance of the catalyst NW. Therefore, it is inferred that the GaP NW is less suitable as an OER catalyst. Moreover, we studied the OER activity of the NW under defected conditions also, and

the trends of the adsorption and Gibbs free energy did not improve, rather they were observed to get much more negative than in the case of pristine NW. Henceforth, we conclude that the GaP NW is not a better candidate for the OER catalyst.

6.4 Conclusion

In summary, the *first-principles* based density functional theory calculations were performed on ultra-thin boron phosphide and gallium phosphide nanowires (NWs) for investigating their ground state structural, electronic and HER/OER catalytic properties. The substitutional doping was introduced in the systems for understanding their effect on the electronic and catalytic profiles of the NWs specifically to determine the methodology for enhancing the catalytic activities (HER and OER) of phosphide nanowires of III-V group. As expected, the imposition of two-dimensional quantum confinement effect results in enhancement of the band gap. In addition, a dramatic indirect to direct band gap transition is observed in both BP and GaP NWs. Apart from the wide-band gap of pristine NWs, substitutional dopants result in reduction in gap magnitude in both cases; for BP NW it changes from 2.96 eV to 2.81 eV for Al-doped NW and to 2.87 eV for Ga-doped NW; whereas, in case of GaP NW, it gets reduced from 3.8 eV to 2.5 eV for both B and N-doped conditions. These results indicate how even a small fraction of foreign element substitution can alter the properties of the NW. Moving towards the final objective of the study, i.e. to investigate the catalytic activities of the phosphide NWs, the overall inspection of the adsorption and Gibbs free energy profiles for BP NW suggests that the BP NW is less preferred for HER catalytic application, and substitutional defect depresses HER activity; on the other hand, the OER activity of the BP NW gets improved on Ga

substitution and indicate site-B to be the most preferred site for oxygen adsorption. In case of GaP NW, the HER activity of the NW is found to be prominent at site-A, with lowest magnitude of energy of adsorption and Gibbs free energy (-1.33 and 1.47 eV). Comparing with the pristine GaP NW (adsorption and Gibbs free energy: -1.53 and -1.29 eV), the B and N doped GaP NWs show contrast results. The NW with B- defect shows lower adsorption and Gibbs free energy (-1.21 and -0.97 eV) while it is observed more in case of N-defected NWs (-1.91 and -1.67 eV). As expected, the ideal catalyst possesses zero Gibbs free energy indicating adsorption and desorption processes feasible, the B-defected NW can be observed as a better HER catalyst among all considered cases, and further enhancement can be achieved by means of tuning the dopant concentration and adsorption surface site engineering. At last, the results of the OER activity of the GaP NW suggest strong binding between the NW surface and oxygen which further increase in case of doped NWs. The too negative magnitude of adsorption and Gibbs free energy of the GaP NW under oxygen adsorption suggest GaP NW to be less suitable for an OER catalyst.

References

(1) McEvoy, J. P.; Gascon, J. A.; Batista, V. S.; Brudvig, G. W. The Mechanism of Photosynthetic Water Splitting. *Photochem. Photobiol. Sci.* **2005**, *4* (12), 940–949. https://doi.org/10.1039/b506755c

(2) Walter, M. G.; Warren, E. L.; McKone, J. R.; Boettcher, S. W.; Mi, Q.; Santori, E. A.; Lewis, N. S. Solar Water Splitting Cells. *Chem. Rev.* **2010**, *110* (11), 6446–6473. https://doi.org/10.1021/cr1002326

(3) Roger, I.; Shipman, M. A.; Symes, M. D. Earth-Abundant Catalysts for Electrochemical and Photoelectrochemical Water Splitting. *Nature Reviews Chemistry*. **2017**, *1(1), 1-13*. https://doi.org/10.1038/s41570-016-0003

(4) Shen, H. J. Thermal-Conductivity and Tensile-Properties of BN, SiC and Ge Nanotubes. *Comput. Mater. Sci.* **2009**, *47* (1), 220–224. https://doi.org/10.1016/j.commatsci.2009.05.027

(5) Bernardini, F.; Fiorentini, V. Spontaneous versus Piezoelectric Polarization in III-V Nitrides: Conceptual Aspects and Practical Consequences. *Phys. Status Solidi Basic Res.* **1999**, *216* (1), 391–398. https://doi.org/10.1002/(SICI)1521-3951(199911)216:1<391::AID-PSSB391>3.0.CO;2-K

(6) Zhang, D.; Zhang, R. Q. Theoretical Prediction on Aluminum Nitride Nanotubes. *Chem. Phys. Lett.* **2003**, *371* (3–4), 426–432. https://doi.org/10.1016/S0009-2614(03)00289-6

(7) Ohno, H.; Chiba, D.; Matsukura, F.; Omiya, T.; Abe, E.; Dietl, T.; Ohno, Y.; Ohtani, K. Electric-Field Control of Ferromagnetism. *Nature* **2000**, *408* (6815), 944–946. https://doi.org/10.1038/35050040

(8) Hasegawa, H.; Akazawa, M. Interface Models and Processing Technologies for Surface Passivation and Interface Control in III-V Semiconductor Nanoelectronics. *Appl. Surf. Sci.* **2008**, *254* (24), 8005–8015. https://doi.org/10.1016/j.apsusc.2008.03.051

(9) Zhang, Y.; Wu, J.; Aagesen, M.; Liu, H. III-V Nanowires and Nanowire Optoelectronic Devices. *Journal of Physics D: Applied Physics*. **2015**, *48*(46), 463001:1-29. https://doi.org/10.1088/0022-3727/48/46/463001

(10) Tsao, J. Y.; Chowdhury, S.; Hollis, M. A.; Jena, D.; Johnson, N. M.; Jones, K. A.; Kaplar, R. J.; Rajan, S.; Van de Walle, C. G.; Bellotti, E.; et al. Ultrawide-Bandgap Semiconductors: Research Opportunities and Challenges. *Advanced Electronic Materials*. **2018**, *4*, 1600501:1-49. https://doi.org/10.1002/aelm.201600501

(11) Standing, A.; Assali, S.; Gao, L.; Verheijen, M. A.; Van Dam, D.; Cui, Y.; Notten, P. H. L.; Haverkort, J. E. M.; Bakkers, E. P. A. M. Efficient Water Reduction with Gallium Phosphide Nanowires. *Nat. Commun.* **2015**, *6*, 7824:1-7. https://doi.org/10.1038/ncomms8824

(12) Chu, S.; Vanka, S.; Wang, Y.; Gim, J.; Wang, Y.; Ra, Y. H.; Hovden, R.; Guo, H.; Shih, I.; Mi, Z. Solar Water Oxidation by an InGaN Nanowire Photoanode with a Bandgap of 1.7 EV. *ACS Energy Lett.* **2018**, *3* (2), 307–314. https://doi.org/10.1021/acsenergylett.7b01138

(13) Zeng, J.; Xu, X.; Parameshwaran, V.; Baker, J.; Bent, S.; Wong, H. S. P.; Clemens, B. Photoelectrochemical Water Oxidation by GaAs Nanowire Arrays Protected with Atomic Layer Deposited NiOx Electrocatalysts. In *Journal of Electronic Materials*; **2018,** 47, 932–937. https://doi.org/10.1007/s11664-017-5824-y

(14) Kibria, M. G.; Nguyen, H. P. T.; Cui, K.; Zhao, S.; Liu, D.; Guo, H.; Trudeau, M. L.; Paradis, S.; Hakima, A. R.; Mi, Z. One-Step Overall Water Splitting under Visible Light Using Multiband InGaN/GaN Nanowire Heterostructures. *ACS Nano* **2013**, *7* (9), 7886–7893. https://doi.org/10.1021/nn4028823

(15) Zhou, B.; Kong, X.; Vanka, S.; Chu, S.; Ghamari, P.; Wang, Y.; Pant, N.; Shih, I.; Guo, H.; Mi, Z. Gallium Nitride Nanowire as a Linker of Molybdenum Sulfides and Silicon for Photoelectrocatalytic Water Splitting. *Nat. Commun.* **2018**, *9* (1), 3856:1-8. https://doi.org/10.1038/s41467-018-06140-1

(16) Dabhi, S. D.; Jha, P. K. Ab Initio Study of Strained Wurtzite InAs Nanowires: Engineering an Indirect-Direct Band Gap Transition through Size and Uniaxial Strain. *RSC Adv.* **2015,** 5, 89993–90000. https://doi.org/10.1039/c5ra16512a

(17) Copple, A.; Ralston, N.; Peng, X. Engineering Direct-Indirect Band Gap Transition in Wurtzite GaAs Nanowires through Size and Uniaxial Strain. *Appl. Phys. Lett.* **2012**, *100* (19), 193108:1-4. https://doi.org/10.1063/1.4718026

(18) Lambert, B.; Le Corre, A.; Toudic, Y.; Lhomer, C.; Grandpierre, G.; Gauneau, M. Electrical and Optical Properties of Rare Earth Dopants (Yb, Er) in n-Type III-V (InP) Semiconductors. *J. Phys. Condens. Matter* **1990**, *2* (2), 479–483. https://doi.org/10.1088/0953-8984/2/2/022

(19) Kohn, W.; Becke, A. D.; Parr, R. G. Density Functional Theory of Electronic Structure. *J. Phys. Chem.* **1996,** 100, 12974-12980. https://doi.org/10.1021/jp960669l

(20) Gajaria, T. K.; Dabhi, S. D.; Jha, P. K. Ab Initio Energetics and Thermoelectric Profiles of Gallium Pnictide Polytypes. *Sci. Rep.* **2019**, *9* (1), 5884:1-20. https://doi.org/10.1038/s41598-019-41982-9

(21) Perdew, J. P.; Zunger, A. Self-Interaction Correction to Density-Functional Approximations for Many-Electron Systems. *Phys. Rev. B* **1981**, *23* (10), 5048–5079. https://doi.org/10.1103/PhysRevB.23.5048

(22) Haas, P.; Tran, F.; Blaha, P. Calculation of the Lattice Constant of Solids with Semilocal Functionals. *Phys. Rev. B - Condens. Matter Mater. Phys.* **2009**, *79* (8), 085104:1-10. https://doi.org/10.1103/PhysRevB.79.085104

(23) Monkhorst, H. J.; Pack, J. D. Special Points for Brillouin-Zone Integrations. *Phys. Rev. B* **1976**, *13* (12), 5188–5192. https://doi.org/10.1103/PhysRevB.13.5188

(24) Grimme, S.; Antony, J.; Ehrlich, S.; Krieg, H. A Consistent and Accurate Ab Initio Parametrization of Density Functional Dispersion Correction (DFT-D) for the 94 Elements H-Pu. *J. Chem. Phys.* **2010**, *132* (15), 154104:1-19. https://doi.org/10.1063/1.3382344

(25) Rupp, C. J.; Chakraborty, S.; Anversa, J.; Baierle, R. J.; Ahuja, R. Rationalizing the Hydrogen and Oxygen Evolution Reaction Activity of Two-Dimensional Hydrogenated Silicene and Germanene. *ACS Appl. Mater. Interfaces* **2016**, *8* (2), 1536–1544. https://doi.org/10.1021/acsami.5b11513

(26) Mir, S. H.; Chakraborty, S.; Jha, P. C.; Wärnå, J.; Soni, H.; Jha, P. K.; Ahuja, R. Two-Dimensional Boron: Lightest Catalyst for Hydrogen and Oxygen Evolution Reaction. *Appl. Phys. Lett.* **2016**, *109* (5), 053903:1-5. https://doi.org/10.1063/1.4960102

(27) Som, N. N.; Mankad, V.; Jha, P. K. Hydrogen Evolution Reaction: The Role of Arsenene Nanosheet and Dopant. *Int. J. Hydrogen Energy* **2018**, *43* (47), 21634–21641. https://doi.org/10.1016/j.ijhydene.2018.03.066

(28) Ustundag, M.; Aslan, M.; Yalcin, B. G. The First-Principles Study on Physical Properties and Phase Stability of Boron-V (BN, BP, BAs, BSb and BBi) Compounds. *Comput. Mater. Sci.* **2014**, *81*, 471–477. https://doi.org/10.1016/j.commatsci.2013.08.056

(29) Assali, S.; Zardo, I.; Plissard, S.; Kriegner, D.; Verheijen, M. A.; Bauer, G.; Meijerink, A.; Belabbes, A.; Bechstedt, F.; Haverkort, J. E. M.; et al. Direct Band Gap Wurtzite Gallium Phosphide Nanowires. *Nano Lett.* **2013**, *13* (4), 1559–1563. https://doi.org/10.1021/nl304723c

(30) Peidong Yang, C. Z. N.; Dou, L.; Yang, P. Bandgap Engineering in Semiconductor Alloy Nanomaterials with Widely Tunable Compositions. *Nature Reviews Materials*. **2017**, *2*, 17070:1-14. https://doi.org/10.1038/natrevmats.2017.70

(31) Hou, D.; Zhang, Y.; Yang, T.; Zhang, J.; Pei, H.; Zhang, J.; Jiang, J.; Li, T. Molecular Structure, Dynamics, and Mechanical Behavior of Sodium Aluminosilicate Hydrate (NASH) Gel at Elevated Temperature: A Molecular Dynamics Study. *Phys. Chem. Chem. Phys.* **2018**, *20* (31), 20695–20711. https://doi.org/10.1039/c8cp03411g

(32) Kumar, V.; Shah, E. V.; Roy, D. R. Electronic Properties of Hexagonal Gallium Phosphide: A DFT Investigation. In *AIP Conference Proceedings*; **2016**, *1731*, 120026:1-3.
